Photoluminescence of Pr3+-doped calcium and strontium stannates

Peer-reviewed author version

STANULIS, Andrius; Katelnikovas, Arturas; VAN BAEL, Marlies; HARDY, An; Kareiva, Aivaras & Jüstel, Thomas (2016) Photoluminescence of Pr3+-doped calcium and strontium stannates. In: JOURNAL OF LUMINESCENCE, 172, p. 323-330.

DOI: 10.1016/j.jlumin.2015.11.021
Handle: http://hdl.handle.net/1942/20813

Luminescence properties of Pr3+-doped calcium and strontium stannates: temperature dependent fluorescence lifetime measurements as a suitable tool for monitoring phase transitions...

ARTICLE *in* JOURNAL OF LUMINESCENCE · NOVEMBER 2015

Impact Factor: 2.72 · DOI: 10.1016/j.jlumin.2015.11.021

6 AUTHORS, INCLUDING:

Marlies Van Bael

Hasselt University

An Hardy

Hasselt University

Aivaras Kareiva

Vilnius University

Thomas Jüstel

Fachhochschule Münster

Author's Accepted Manuscript

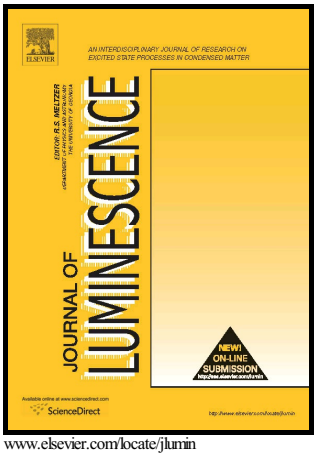

www.elsevier.com/locate/jlumin

Luminescence properties of Pr^{3+}-doped calcium and strontium stannates: temperature dependent fluorescence lifetime measurements as a suitable tool for monitoring phase transitions of optically active materials

Andrius Stanulis, Arturas Katelnikovas, Marlies Van Bael, An Hardy, Aivaras Kareiva, Thomas Justel

PII: S0022-2313(15)30109-5
DOI: http://dx.doi.org/10.1016/j.jlumin.2015.11.021
Reference: LUMIN13720

To appear in: *Journal of Luminescence*

Received date: 16 June 2015
Revised date: 10 November 2015
Accepted date: 17 November 2015

Cite this article as: Andrius Stanulis, Arturas Katelnikovas, Marlies Van Bael, An Hardy, Aivaras Kareiva and Thomas Justel, Luminescence properties of Pr^{3+} doped calcium and strontium stannates: temperature dependent fluorescenc lifetime measurements as a suitable tool for monitoring phase transitions o optically active materials, *Journal of Luminescence* http://dx.doi.org/10.1016/j.jlumin.2015.11.021

Luminescence properties of Pr^{3+}-doped calcium and strontium stannates: temperature dependent fluorescence lifetime measurements as a suitable tool for monitoring phase transitions of optically active materials.

Andrius Stanulis[a,b,*], Arturas Katelnikovas[c], Marlies Van Bael[d,e], An Hardy[d,e], Aivaras Kareiva[a], and Thomas Justel[f,*]

[a]*Department of Inorganic Chemistry, Vilnius University, Naugarduko 24, LT-03225 Vilnius, Lithuania*
[b]*Center for Physical Sciences and Technology, Department of Electrochemical Materials Sciences, A. Gostauto 9, LT-01108 Vilnius, Lithuania*
[c]*Department of Analytical and Environmental Chemistry, Vilnius University, Naugarduko 24, LT-03225 Vilnius, Lithuania*
[d]*Institute for Materials Research, Laboratory of Inorganic and Physical Chemistry, Hasselt University, Agoralaan D, B-3590 Diepenbeek, Belgium*
[e]*IMEC, division IMOMEC, Agoralaan D, B-3590 Diepenbeek, Belgium*
[f]*Department of Chemical Engineering, Münster University of Applied Sciences, Stegerwaldstr. 39, D-48565 Steinfurt, Germany*

Abstract

A series of Pr^{3+}-doped $CaSnO_3$, $SrSnO_3$ and Ca_2SnO_4 samples were prepared by a conventional high temperature solid-state reaction route. All samples were characterized by powder X-ray diffraction (XRD) analysis, photoluminescence (PL), photoluminescence thermal quenching (TQ) and fluorescence lifetime (FL) measurements. Moreover, luminous efficacies (LE) and color points according to the CIE 1931 color space diagram were calculated and discussed. The incorporation of Pr^{3+} ions into $CaSnO_3$ and $SrSnO_3$ host materials results in intense white luminescence, which originates from the mixture of green, orange and red emissions. Temperature dependent luminescence lifetime measurements of $SrSnO_3$:Pr^{3+} phosphor showed abnormalities near 180 and 260 K, which confirm the existence of a low temperature structural phase transitions in $SrSnO_3$. Pr^{3+}-doped Ca_2SnO_4 phosphor emits intense

red light upon excitation. Therefore, efficient UV excitation brands $Ca_2SnO_4:Pr^{3+}$ as an attractive phosphor for application in phosphor converted solid state light sources.

Keywords: stannates, doping, trivalent praseodymium, photoluminescence, structural phase transitions

*Corresponding author: E-mail: andrius.stanulis@chf.vu.lt

1. Introduction

Perovskite-type alkaline earth metal meta-stannates with the general formula of $MSnO_3$ (M = Ca, Sr and Ba) have received increasing attention due to their wide applications in ceramic dielectric bodies [1, 2], gas and humidity sensors [3-5], anode materials for lithium ion batteries [6-10] and photocatalysts [11-17]. However, luminescent materials with perovskite-related structures have not been extensively studied yet. Therefore, the realisation of intensively luminescent perovskite-related oxides might lead to novel attractive materials for the future development of multifunctional devices [18]. The main feature that makes perovskites versatile for chemical tuning of composition is the simplicity of their crystal structure, which is of great assistance in interpreting the experimental results and hence clarifying the luminescence mechanisms.

During the last decade, alkaline earth ortho-stannates (M_2SnO_4, M = Ca, Sr, and Ba) have been extensively studied as host materials for new luminescent materials due to their rigid crystal structure type and thus rather high physical and chemical stability [19]. Incorporation of optically active lanthanide ions into the stannate host matrixes resulted in phosphors possessing photoluminescent [20-22] and long lasting phosphorescent (LLP) [23-25] properties.

So far, Pr^{3+} and Tb^{3+}-doped $MSnO_3$ (M = Ca and Sr) perovskites have been developed as white and green light emitting phosphors, respectively [26-28]. Lu et al. [29] studied the luminescent properties of Eu^{3+}-doped $MSnO_3$ (M = Ca, Sr and Ba) phosphors and revealed that red emission of $CaSnO_3$:Eu^{3+} is twice stronger than Eu^{3+}-doped $SrSnO_3$ and $BaSnO_3$. This was ascribed to the orthorhombically distorted $CaSnO_3$:Eu^{3+} crystal structure with reduced symmetry at the Ca^{2+}/Eu^{3+} sites in comparison to cubic $BaSnO_3$:Eu^{3+}, wherein Eu^{3+} ions occupy sites with a larger symmetry.

It is well known that luminescence measurements are very sensitive to monitor variations in the chemical and structural local environment of respective luminescent ions and thus have the potential to probe distortions of fluorescence sites. Luminescence efficiency, emission spectra and excited state lifetimes are factors that are influenced by the type of crystalline structure, pressure and temperature. Discontinuous changes in these photoluminescence governing parameters occur during phase transitions of insulating materials while simultaneously exciting and heating or cooling the samples [30, 31]. However, there was no report on the detection of a phase transition in alkaline earth stannates by utilizing emission lifetime measurements so far.

In the framework of this work we investigated the photoluminescence properties of Pr^{3+}-doped $CaSnO_3$, $SrSnO_3$, and Ca_2SnO_4 samples prepared by solid-state reactions. The influence of the Pr^{3+} concentration on the peculiarities of the phase formation and on the photoluminescence is discussed. Particular emphasis is given to $SrSnO_3$ sample doped by 4% Pr^{3+}, which showed discontinuities in luminescence lifetimes corresponding to the structural phase transition.

2. Experimental

2.1 Synthesis of $CaSnO_3:Pr^{3+}$, $SrSnO_3:Pr^{3+}$ and $Ca_2SnO_4:Pr^{3+}$

Praseodymium-doped meta- and ortho-stannate μ-scale powder samples were synthesized by traditional a solid state reaction method. Stoichiometric amounts of high purity raw materials ($CaCO_3$ (≥99.995% Aldrich), $SrCO_3$ (≥99.9% Aldrich), SnO_2 (≥99% Merck) and $Pr_2(C_2O_4)_3{\cdot}10H_2O$ (≥99%, Merck)) were thoroughly mixed in an agate mortar using acetone as a grinding media. The mixture of starting materials were dried, transferred to an alumina crucible and annealed at 1200 and 1400 °C for 10 h in air in order to obtain single phase meta- and ortho-stannate samples, respectively. A series of phosphors with a dopant concentration ranging from 0.1 to 4 mol % of Ca^{2+} and Sr^{2+}ions were prepared. The undoped $SrSnO_3$ host material was obtained in the same way just without adding a Pr^{3+} source.

2.2 Characterization

Powder X-ray diffraction (XRD) analysis has been carried out by employing a Rigaku MiniFlex II diffractometer working in the Bragg–Brentano (θ/2θ) geometry. The data were collected within 2θ angle from 10° to 80° at a step of 0.02° and integration time of 1 s using Ni-filtered Cu Kα line.

Excitation (excitation slit 0.5 nm and emission slit 1.5 nm) and emission (excitation slit 5.0 nm and emission slit 0.5 nm) spectra were recorded in the ranges 250 – 550 and 500 – 800 nm, respectively, on an Edinburgh Instruments FSL900 fluorescence spectrometer equipped with a 450 W Xe arc lamp, mirror optics for powder samples and a Peltier cooled (-20 °C) single-photon counting photomultiplier (Hamamatsu R2658P). The photoluminescence emission spectra were corrected by using a correction file obtained from a calibrated tungsten

incandescent lamp certified by the NPL (National Physics Laboratory, UK) and excitation spectra were corrected by a reference detector.

Reflection spectra were recorded on the same spectrometer type equipped with an integration sphere coated with barium sulfate. $BaSO_4$ (99% Sigma-Aldrich) was used as a reflectance standard.

Decay curves were recorded with an Edinburgh Instruments FL920 lifetime spectrometer equipped with an Edinburgh Instruments μF900 flash lamp and a Hamamatsu extended red sensitivity photomultiplier tube. Data was acquired in a gated single photon counting (MCS) mode. All measurements were performed at room temperature in air.

For thermal quenching (TQ) measurements a cryostat ''MicrostatN'' from Oxford Instruments has been applied to the present spectrometer. Liquid nitrogen was used as a cooling agent. Measurements were carried out from 100 to 500 K in 20 or 50 K steps.

3. Results and discussion

3.1 Crystal structures of $MSnO_3$ (M = Ca, Sr, Ba) and Ca_2SnO_4

Solid state compounds belonging to the perovskite type have in general the formula ABO_3 where the sum of the cation valencies is 6. $BaSnO_3$ crystallizes in an ideal cubic crystal structure with the space group *Pm3m* (#221) [32]. This structure consists of a vertex-sharing SnO_6 octahedral framework with the barium ions filling the cubo-octahedral cavities (CN = 12) in the structure, as shown in Figure 1c. An additional four barium atoms surround each oxygen in a plane perpendicular to the Sn-O-Sn bond, but the Sn–O distances (2.055 Å) are much shorter than the Ba–O distances (2.905Å) [33].

If Ba^{2+} is replaced by Ca^{2+} or Sr^{2+}, two main types of deformation are possible, and may occur separately or at the same time [34]. Firstly, the unit cell shape is changing by altering either the relative lengths of the cell-edges or the axial angle. Secondly, if the atomic parameters of some or all of the atoms are slightly altered then slight displacement in any direction involves a lowering of the symmetry and also, in general, a doubling of at least one cell edge. On the other hand, a doubled cell edge implies that atomic parameters are different from those of the ideal structure.

The crystal structures of $CaSnO_3$ and $SrSnO_3$ were first solved by Vegas et al. in 1986 [35] and are shown in Figure 1a and b, respectively. In $CaSnO_3$ and $SrSnO_3$ the local octahedral environment around Sn^{4+} ion is maintained and the vertex-sharing octahedral connectivity of the perovskite structure is also preserved, but the octahedral tilting leads to significant changes in the local environment around the A-site cation (Ca or Sr) as well as oxygen. $CaSnO_3$ and $SrSnO_3$ are both distorted from ideal cubic into the orthorhombic structure with *Pnma* (#62) symmetry by an octahedral tilting distortion, which is driven by a mismatch in the fit of the alkaline earth cation to the cubo-octahedral cavity in the vertex-sharing octahedral network due to the smaller ionic radius of Sr^{2+} or Ca^{2+} than Ba^{2+}. The average Sn–O distance and the octahedral configuration around tin are relatively insensitive to substitutions on the A-site. However, the Sn–O–Sn bond is increasingly distorted from linearity if the size of cation in A-site decreases. Such a distortion in the nonlinear Sn–O–Sn bond is expected to have a great influence on the migration of charge carriers and delocalization of excited energy and thus on photophysical and photocatalytic properties of stannates [33, 36].

The crystal structure of Ca_2SnO_4 belongs to the Sr_2PbO_4-type structure with an orthorhombic unit cell and space group *Pbam* (#55). In this structure type, Ca atoms occupy a 4h site (x, y, 1/2)

and are coordinated by seven oxygen atoms, whereas Sn atoms occupy a 2a site (0, 0, 0) and are coordinated by six oxygen atoms [37, 38]. The SnO_6 octahedra are linked by sharing edges with each other forming one-dimensional chains in Ca_2SnO_4 [21], as shown in Figure 1d.

3.2 Powder X-ray diffraction analysis

The XRD pattern of the $CaSnO_3$:4% Pr^{3+}sample together with the standard data of $CaSnO_3$ (ICDD#04-015-3326) are shown in Figure 2a. The obtained results demonstrate that Pr^{3+} ions do not have significant influence on the crystal structure at low concentration. However, the existence of two secondary phases, namely $Pr_2Sn_2O_7$ (ICDD#00-087-1219) and SnO_2 (ICDD#00-077-0450) was detected, when dopant concentration reached 4 mol-%.

The XRD pattern of Pr^{3+}-doped $SrSnO_3$ specimen is illustrated in Figure 2b. The diffraction peaks of the sample are well consistent with the standard data of $SrSnO_3$ (ICDD#04-010-2598). The presence of trace impurities in 4 mol-% doped $SrSnO_3$ sample indicates that the solubility of Pr^{3+} ions in this host material is better in comparison to $CaSnO_3$.

Figure 2c represents the powder XRD pattern of Ca_2SnO_4:4% Pr^{3+} phosphor. All the peaks of synthesized sample match well with Bragg reflections of the reference pattern of Ca_2SnO_4 (ICDD#04-008-2918). The phase analysis revealed that the Pr^{3+} ions completely dissolved in the Ca_2SnO_4 host lattice. The unavoidable presence of calcium meta-stannate phase was detected in all samples, as well as in the undoped host material.

3.3 Optical properties

Figure 3 shows the excitation, emission and diffuse reflectance spectra of $CaSnO_3$:1% Pr^{3+}, $SrSnO_3$:4% Pr^{3+} and Ca_2SnO_4:0.25% Pr^{3+}, respectively. The excitation spectrum of $CaSnO_3$:1% Pr^{3+} (Figure 3a) and $SrSnO_3$:4% Pr^{3+} (Figure 3b) exhibit broad bands in between

250 and 320 nm. These bands are attributed to the band gap absorption of the host lattice (HL). The excitation peaks of $CaSnO_3:Pr^{3+}$ and $SrSnO_3:Pr^{3+}$ are centered at 265 and 290 nm, respectively. In fact, Pr^{3+} doped $BaSnO_3$ samples were also prepared, however, they have not shown any photoluminescence.

The emission spectrum of Pr^{3+} doped $CaSnO_3$ sample was measured upon excitation at 265 nm at ambient temperature and is depicted in Figure 3a. It consists of five major emission lines peaking at around 488, 530, 613, 656 and 742 nm that are assigned to the intraconfigurational 4f-4f transitions, viz. $^3P_0 \rightarrow {}^3H_4$, $^3P_0 \rightarrow {}^3H_5$, $^1D_2 \rightarrow {}^3H_4$, $^3P_0 \rightarrow {}^3F_2$ and $^3P_0 \rightarrow {}^3F_4$ typicall for the $[Xe]4f^2$ configuration of Pr^{3+} ions, respectively [39]. The emission spectra of $SrSnO_3$:4% Pr^{3+} (Figure 3b) excited at 290 nm is quite similar to those of $CaSnO_3$:1% Pr^{3+}. However, the characteristic emission lines of $SrSnO_3$:4% Pr^{3+} phosphor are slightly shifted towards higher energy. The most intense emission peaks are located in the green (500 nm), orange (600 nm) and red (660 nm) spectral regions. Such mixture of complementary colors caused white coloration in the Pr^{3+} doped $CaSnO_3$ and $SrSnO_3$ samples [26, 28].

The excitation spectrum of 0.25 mol-% Pr^{3+} doped Ca_2SnO_4 phosphor monitored for 622.5 nm emission is depicted in Figure 3c. The excitation spectra can be divided into two main sections. The first one is in the range of 250 – 370 nm with two strong broad bands situated at 258 and 310 nm respectively, which can be ascribed to the $[Xe]4f^2 - [Xe]4f^15d^1$ interconfigurational transitions of Pr^{3+} [40]. The asymmetric band shape with maximum at 258 nm is due to the fact, that it is overlapped with the absorption of host lattice. The second one is in the spectral range from 400 to 520 nm with several sharp peaks, which are attributed to intraconfigurational 4f – 4f transitions of Pr^{3+} ions from the ground state $^3H_4$ to excited ^3P_J ($J = 0$, 1, 2) and $^1I_6$ states. [41, 42].

The interconfigurational transition from the ground state $[Xe]4f^2$ configuration to the $[Xe]4f^15d^1$ state is almost equal in intensity to the 4f-4f intraconfigurational $^3H_4 \rightarrow {}^3P_0$ transition at 496 nm. The emission spectra of Ca_2SnO_4:0.25% Pr^{3+} sample (Figure 3c) consists of four emission line multiplets at 604, 622.5, 656, and 718 nm, which can be ascribed to $^1D_2 \rightarrow {}^3H_4$, $^3P_0 \rightarrow {}^3H_6$, $^3P_0 \rightarrow {}^3F_2$, and $^3P_0 \rightarrow {}^3F_4$ transitions, respectively. It also worth mentioning that the Ca_2SnO_4:Pr^{3+} samples showed very weak to no luminescence in the cyan range, viz. between 480 and 500 nm which is in contrast to their $CaSnO_3$:Pr^{3+} and $SrSnO_3$:Pr^{3+} counterparts.

The emission spectra of Ca_2SnO_4:Pr^{3+} phosphor under different excitation wavelengths (310 and 496 nm) revealed that emission intensity is two times stronger if the excitation takes place at 310 nm. Therefore, the efficiency of UV excitation makes the phosphor more attractive for application in fluorescent light sources with a primary radiation source emitting in the UV range.

Reflection spectra of Pr^{3+} doped $SrSnO_3$ sample (Figure 3b) exhibits a broad absorption band ranging from 250 to 350 nm, which can be attributed to the typical optical response of a wide band gap semiconductor. The optical band gap of $SrSnO_3$ as reported in literature is 4.1 eV [15]. Generally, in rather covalent oxides such as $SrTiO_3$, $BaTiO_3$, and anatase-type TiO_2, the strong coupling between electrons and lattice vibrations can lead to the formation of self-trapped excitons (STEs), whose recombination usually gives rise to a broad band and unstructured and broad visible emission with a rather large Stokes shift [43-45].

The excitation (λ_{em} = 550 nm) and emission (λ_{ex} = 254 nm) spectra of undoped $SrSnO_3$ sample are shown in Figure 4. It is obvious that the broad emission spectrum originates from a multiphoton process, where several STE states are formed inside the band gap, allowing numerous different energetic transitions among them. As a result, a broad band covering a large part of the visible range can be observed for the $SrSnO_3$ host material [46]. The calculated

CIE 1931 color space coordinate for undoped $SrSnO_3$ emission is (x = 0.354 and y = 0.454), which is located on the border between the green and white colour space.

Figure 5 shows the emission intensity integrals as a function of Pr^{3+} concentration in alkaline earth meta- and ortho-stannates. The photoluminescence intensity of Pr^{3+} doped $CaSnO_3$ sample under 265 nm excitation rapidly increases up to 2 mol-% and then slightly decreases if the dopant concentration reaches 4 mol-%. The emission intensity integral of $SrSnO_3$:Pr^{3+} phosphor increases steeply at low concentration region up to 1 mol-% and then continuously increases up to 4 mol-% without reaching the maximum value. The possible explanation for the absence of concentration quenching is that the solubility limit of Pr^{3+} in the $SrSnO_3$ host material was not reached and that the average Pr^{3+}-Pr^{3+} distance is too large for efficient energy transfer. Dependencies of the emission intensity integral on Pr^{3+} ion concentration in Ca_2SnO_4 host material follow the same trend, if different excitation wavelengths are used. The luminescence intensity increases with Pr^{3+} concentration until a maximum intensity of 0.25 mol-% is reached and then the emission intensity declines quickly due to the concentration quenching effect.

An interesting behavior can be observed for the concentration dependent emission spectra of $SrSnO_3$:Pr^{3+} in the 500 to 600 nm range as plotted in Figure 6. The STE emission intensity increases with increased Pr^{3+} content up to 1 mol-%. At the same time the characteristic transition at 528 nm of Pr^{3+} ion starts to appear and increases in intensity. Consequently, $^3P_0 \rightarrow {}^3H_5$ transition becomes prominent while STE emission diminishes, when activator concentration reaches 4 mol-%.

Figure 7 depicts the thermal quenching of photoluminescence and temperature dependent decay time data of $CaSnO_3$:1% Pr^{3+} sample under 265 nm excitation. The integral light output

increases by 50% in the temperature range from 150 to 350 K and then starts to decrease with a further temperature increase (Figure 7a).

The temperature dependent PL emission intensity integrals of $SrSnO_3$:4% Pr^{3+} excited at 290 nm are depicted in Figure 8a. Taking into account that integral values have shifted towards lower temperature region by ~150 K, the tendency has remained unchanged.

In general, the emission intensity decreases with raising temperature of the phosphor. However, an opposite effect was observed for $CaSnO_3$:1% Pr^{3+} and $SrSnO_3$:4% Pr^{3+} up to 350 and 200 K, respectively. This can be explained by the occurrence of thermally stimulated luminescence. According to Clabau et al., the trap depth is proportional to the strength of the anion-cation bonds of the host lattice [47]. In $MSnO_3$ phosphors, the trap depth is determined by the strength of M–O bond. Since electronegativity of Ca is higher than that of Sr, the strength of Ca–O bond increases as well. Therefore, the depth (energy) of the hole traps should be $Sr^{2+} < Ca^{2+}$. This effect can be observed comparing both temperature dependent emission integrals plotted in Figure 7a and Figure 8a.

The energy stored within the host lattice is being released most efficiently in $CaSnO_3$:1% Pr^{3+} and $SrSnO_3$:4% Pr^{3+} phosphors at 350 and 200 K, respectively. A Boltzmann fit was applied to calculate $TQ_{1/2}$ value. The fit resulted in $TQ_{1/2}$ values with a larger error for $CaSnO_3$:1% Pr^{3+} sample (490±40 K) than those for $SrSnO_3$:4% Pr^{3+} (387±14 K).

The temperature dependent decay curves of $CaSnO_3$:1% Pr^{3+} and $SrSnO_3$:4% Pr^{3+} phosphors were fitted by a tri-exponential decay function. The decay time value τ_3 of $CaSnO_3$:1% Pr^{3+} sample gradually increases until reaches maximum value of 0.6 ms at 400 K and then abruptly decreases upon an increase in temperature (Figure 7b).

The temperature dependent decay time values of $SrSnO_3$:4% Pr^{3+} sample are plotted in Figure 8b. The octahedral tilting leads to an increase of the distances between oxygen and Pr^{3+} at 180 and 260 K. As a result the band gap decreases so that photoionisation of the excited Pr^{3+} becomes more pronounced, which causes the decline of the photoluminescence intensity.

It is evident that the third exponential decay component (τ_3) show low temperature anomalies with two minima points close to 180 and 260 K. The observed abrupt lifetime decrease can be explained by occurring phase transition as a result of changing in the Sr^{2+}/Pr^{3+} local surrounding. To our knowledge only Kotan et al. have reported the anomalies in the PL spectra of $SrSnO_3$:Tb^{3+} compatible with a structural phase transition at about 260 K [48].

For the first time low temperature anomalies in the Raman spectra, dielectric response and differential thermal analysis of strontium stannate ceramics were discovered by Singh et al. [1]. The author claimed that transition at 160 K may be second order and is likely causes by a displacement due to octahedral tilting, while the phase transition near 265 K appears to be an order–disorder one. Singh et al. proposed that such low temperature phase transitions were not predicted and are unexpected for this perovskite, indicating the need for further study of $SrSnO_3$ at low temperatures, by additional structural methods. Therefore, temperature dependent fluorescence lifetime measurements are particularly suitable for monitoring phase transition of optically active materials.

The temperature dependent emission intensity integrals and lifetime values of Ca_2SnO_4:0.25% Pr^{3+} sample are shown in Figures 9a and 9b, respectively.

It is obvious that the integral light output of the phosphor decrease if the temperature is increased. A Boltzmann sigmoidal fit was used for the calculation of $TQ_{1/2}$ value. The estimated $TQ_{1/2}$ value for Ca_2SnO_4:0.25% Pr^{3+} specimen with greater error (573±20 K) is due to the fact

that emission integrals do not decrease to half of its low temperature value. The mono-exponential decay time values show an analogue tendency that decreases with increasing temperature. This clearly demonstrates that both external and internal efficiency of the phosphor decreases with increasing temperature.

Pr^{3+} concentration dependent decay curves of Pr^{3+}-doped different stannate phosphors are given in Figure 10.

As observed, the decay curves or decay constants of the samples are quite different from each other, again suggesting different internal quantum efficiency. Especially, the original behavior of decay constant is observed for $Ca_2SnO_4:Pr^{3+}$ phosphor.

Figure 11 shows the chromaticity coordinates of $CaSnO_3:Pr^{3+}$, $SrSnO_3:Pr^{3+}$ and $Ca_2SnO_4:Pr^{3+}$ samples, respectively. With increasing Pr^{3+} concentration, the *x* value increases and the *y* value decreases. However, comparing the three host materials with each other, in concentration range from 0.1 to 4 mol % of Pr^{3+}, the color points are shifted between different matrices.

Conclusions

The photoluminescence properties of $CaSnO_3:Pr^{3+}$, $SrSnO_3:Pr^{3+}$ and $Ca_2SnO_4:Pr^{3+}$ samples synthesized via a solid-state reaction route were investigated in this study. The emission spectrum of Pr^{3+} doped $CaSnO_3$ sample consists of five major emission lines peaking at around 488, 530, 613, 656 and 742 nm and are assigned to intraconfiguration transitions $^3P_0 \rightarrow {}^3H_4$, $^3P_0 \rightarrow {}^3H_5$, $^1D_2 \rightarrow {}^3H_4$, $^3P_0 \rightarrow {}^3F_2$ and $^3P_0 \rightarrow {}^3F_4$ states of the $[Xe]4f^2$ configuration for Pr^{3+} ions, respectively. The emission spectra of $SrSnO_3:Pr^{3+}$ phosphor is quite similar to $CaSnO_3:Pr^{3+}$ sample. The most intense emission peaks are located in the green (500 nm), orange (600 nm), and red (660 nm) spectral region. The emission spectra of $Ca_2SnO_4:Pr^{3+}$ phosphor under different excitation wavelengths revealed, that its efficiency upon UV excitation is attractive for

application in phosphor converted LEDs. The concentration quenching effect was studied by varying the Pr^{3+} concentration in each matrix.

The decay curves and decay constants of the samples are quite different from each other, again suggesting a different internal quantum efficiency of the activator ion. In particular, the original behavior of decay speed is observed for $SrSnO_3:Pr^{3+}$ phosphor in the temperature range from 100 to 300 K.

Finally, the temperature dependent fluorescence lifetime measurements of $SrSnO_3:Pr^{3+}$ sample demonstrated that these measurements are useful for monitoring phase transitions of optically active materials.

References

[1] M.K. Singh, J.W. Hong, N.K. Karan, H.M. Jang, R.S. Katiyar, S.A.T. Redfern, J.F. Scott, J. Phys-Condens. Matter. 22 (2010) 095901.
[2] P. Singh, B.J. Brandenburg, C.P. Sebastian, S. Singh, D. Kumar, O. Parkash, Jpn. J. Appl. Phys. 47 (2008) 3540-3545.
[3] S.W. Tao, F. Gao, X.Q. Liu, O.T. Sorensen, Sens. Actuator B-Chem. 71 (2000) 223-227.
[4] J. Cerda, J. Arbiol, G. Dezanneau, R. Diaz, J.R. Morante, Sens. Actuator B-Chem. 84 (2002) 21-25.
[5] H. Cheng, Z.G. Lu, Solid State Sci. 10 (2008) 1042-1048.
[6] N. Sharma, K.M. Shaju, G.V.S. Rao, B.V.R. Chowdari, J. Power Sources 139 (2005) 250-260.
[7] Y. Sharma, N. Sharma, G.V.S. Rao, B.V.R. Chowdari, Chem. Mater. 20 (2008) 6829-6839.
[8] S. Zhao, Y. Bai, W.F. Zhang, Electrochim. Acta 55 (2010) 3891-3896.
[9] C. Li, Y.Q. Zhu, S.M. Fang, H.X. Wang, Y.H. Gui, L. Bi, R.F. Chen, J. Phys. Chem. Solids 72 (2011) 869-874.
[10] M. Mouyane, M. Womes, J.C. Jumas, J. Olivier-Fourcade, P.E. Lippens, J. Solid State Chem. 184 (2011) 2877-2886.
[11] P.H. Borse, J.S. Lee, H.G. Kim, J. Appl. Phys. 100 (2006) 124915.
[12] P.H. Borse, U.A. Joshi, S.M. Ji, J.S. Jang, J.S. Lee, E.D. Jeong, H.G. Kim, Appl. Phys. Lett. 90 (2007) 034103.
[13] Y.P. Yuan, J. Lv, X.J. Jiang, Z.S. Li, T. Yu, Z.G. Zou, J.H. Ye, Appl. Phys. Lett. 91 (2007) 094107.
[14] C.W. Lee, D.W. Kim, I.S. Cho, S. Park, S.S. Shin, S.W. Seo, K.S. Hong, Int. J. Hydr. Energy 37 (2012) 10557-10563.
[15] W.F. Zhang, J.W. Tang, J.H. Ye, Chem. Phys. Lett. 418 (2006) 174-178.
[16] D. Chen, J.H. Ye, Chem. Mater. 19 (2007) 4585-4591.
[17] B. Bellal, B. Hadjarab, A. Bouguelia, M. Trari, Theor. Exp. Chem. 45 (2009) 172-179.

[18] K. Ueda, T. Yamashita, K. Nakayashiki, K. Goto, T. Maeda, K. Furui, K. Ozaki, Y. Nakachi, S. Nakamura, M. Fujisawa, T. Miyazaki, Jpn. J. Appl. Phys. 45 (2006) 6981.
[19] R.C. Ropp, Luminescence and the Solid State, Elsevier Science, 2004.
[20] H.M. Yang, J.X. Shi, M.L. Gong, J. Solid State Chem. 178 (2005) 917-920.
[21] T. Yamashita and K. Ueda, J. Solid State Chem. 180 (2007) 1410-1413.
[22] H.M. Yang, J.X. Shi, M.L. Gong, J. Alloys Compd. 415 (2006) 213-215.
[23] Y. Jin, Y. Hu, L. Chen, X. Wang, G. Ju, Z. Mu, J. Lumin. 138 (2013) 83-88.
[24] B. Lei, H. Zhang, W. Mai, S. Yue, Y. Liu, S.-Q. Man, Solid State Sci. 13 (2011) 525-528.
[25] X. Yu, X. H. Xu, J. B. Qiu, Mater. Res. Bull. 46 (2011) 627-629.
[26] T. Nakamura, M. Shima, M. Yasukawa, K. Ueda, J. Sol-Gel Sci. Technol. 61 (2012) 362-366.
[27] Z. Liu, Y. Liu, Mater. Chem. Phys. 93 (2005) 129-132.
[28] K. Goto, Y. Nakachi, K. Ueda, Thin Solid Films 516 (2008) 5885-5889.
[29] Z. Lu, L. Chen, Y. Tang, Y. Li, J. Alloys Compd. 387 (2005) L1-L4.
[30] P.D. Townsend, M. Maghrabi, B. Yang, Nucl. Instr. Meth. Phys. Res. B 191 (2002) 767-771.
[31] P.D. Townsend, B. Yang, Y. Wang, Contemp. Phys. 49 (2008) 255-280.
[32] A.J. Smith, A.J.E. Welch, Acta Crystallogr. 13 (1960) 653-656.
[33] H. Mizoguchi, H.W. Eng, P.M. Woodward, Inorg. Chem. 43 (2004) 1667-1680.
[34] D.M. Helen, Proc. Phys. Soc. 58 (1946) 133.
[35] A. Vegas, M. Vallet-Regi, J.M. Gonzalez-Calbet, M.A. Alario-Franco, Acta Crystallogr. Sect. B 42 (1986) 167-172.
[36] W. Zhang, J. Tang, J. Ye, J. Mater. Res., 2007, 22, 1859-1871.
[37] M. Trömel, Z. Anorg. Allg. Chem. 371 (1969) 237-247.
[38] H. Yamane, Y. Kaminaga, S. Abe, T. Yamada, J. Solid State Chem. 181 (2008) 2559-2564.
[39] A. Katelnikovas, H. Bettentrup, D. Dutczak, A. Kareiva, T. Jüstel, J. Lumin. 131 (2011) 2754-2761.
[40] W. Jia, A. Pérez-Andújar, I. Rivera, J.Electrochem. Soc. 150 (2003) H161-H164.
[41] Y. Jin, Y. Hu, L. Chen, X. Wang, G. Ju, Opt. Mater. 35 (2013) 1378-1384.
[42] X. Yu, X.H. Xu, S.Y. Xin, J.B. Qiu, J. Am. Ceram. Soc. 94 (2011) 985-987.
[43] R. Leonelli, J.L. Brebner, Phys. Rev. B 33 (1986) 8649-8656.
[44] N. Hosaka, T. Sekiya, S. Kurita, J. Lumin. 72-74 (1997) 874-875.
[45] K. Wakabayashi, Y. Yamaguchi, T. Sekiya, S. Kurita, J. Lumin. 112 (2005) 50-53.
[46] J. Bohnemann, R. Libanori, M.L. Moreira, E. Longo, Chem. Eng. J. 155 (2009) 905-909.
[47] F. Clabau, X. Rocquefelte, T. Le Mercier, P. Deniard, S. Jobic, M.H. Whangbo, Chem. Mater. 18 (2006) 3212-3220.
[48] Z. Kotan, M. Ayvacikli, Y. Karabulut, J. Garcia-Guinea, L. Tormo, A. Canimoglu, T. Karali, N. Can, J. Alloys Compd. 581 (2013) 101-108.

Fig. 1. Crystal structure of (a) $CaSnO_3$, (b) $SrSnO_3$, (c) $BaSnO_3$ and (d) Ca_2SnO_4 along the c-axis.

Fig. 2. Powder XRD patterns of (a) $CaSnO_3$:4% Pr^{3+} (b) $SrSnO_3$:4% Pr^{3+}, and (c) Ca_2SnO_4:4% Pr^{3+}.

Fig. 3. Excitation, emission and reflection spectra of (a) $CaSnO_3$:1% Pr^{3+} (b) $SrSnO_3$:4% Pr^{3+}, and (c) Ca_2SnO_4:0.25% Pr^{3+}.

Fig. 4. Photoluminescence excitation and emission spectra of undoped $SrSnO_3$ (the inset picture shows a digital image of $SrSnO_3$ excited upon 254 nm).

Fig. 5. Emission intensity integrals as a function of Pr^{3+} concentration in different alkaline earth stannate phosphors.

Fig. 6. Emission spectra of $SrSnO_3$ as a function of Pr^{3+} concentration.

Fig. 7. Normalized emission integrals (a) and emission decay constants (b) as a function of temperature of the $CaSnO_3$:1% Pr^{3+} sample.

Fig. 8. Normalized emission integrals (a) and emission decay constants (b) as a function of temperature of the $SrSnO_3$:4% Pr^{3+} sample.

Fig. 9. Normalized emission integrals (a) and emission decay values (b) as a function of temperature of the Ca_2SnO_4:0.25% Pr^{3+} sample.

Fig. 10. Decay curves of (a) $CaSnO_3$:Pr^{3+}, (b) $SrSnO_3$:Pr^{3+} and (c) Ca_2SnO_4:Pr^{3+} as a function of Pr^{3+} concentration.

Fig. 11. CIE1931 color coordinates of $CaSnO_3$:Pr^{3+} (a), $SrSnO_3$:Pr^{3+} (b) and Ca_2SnO_4:Pr^{3+} (c) with different Pr^{3+} concentrations. Exact color points and lumen equivalent values for each Pr^{3+} concentration are given in the inset tables. The insets also show the digital images of the respective compounds excited at 254 nm.

Pr^{3+}, mol-%	QE, %	
	$CaSnO_3$	$SrSnO_3$
	λ_{ex} = 265 nm	λ_{ex} = 280 nm
0.1	1.61	4.66
0.25	2.69	7.23
0.5	3.72	13.39
1	8.66	17.27
2	10.79	22.98
4	11.82	22.15

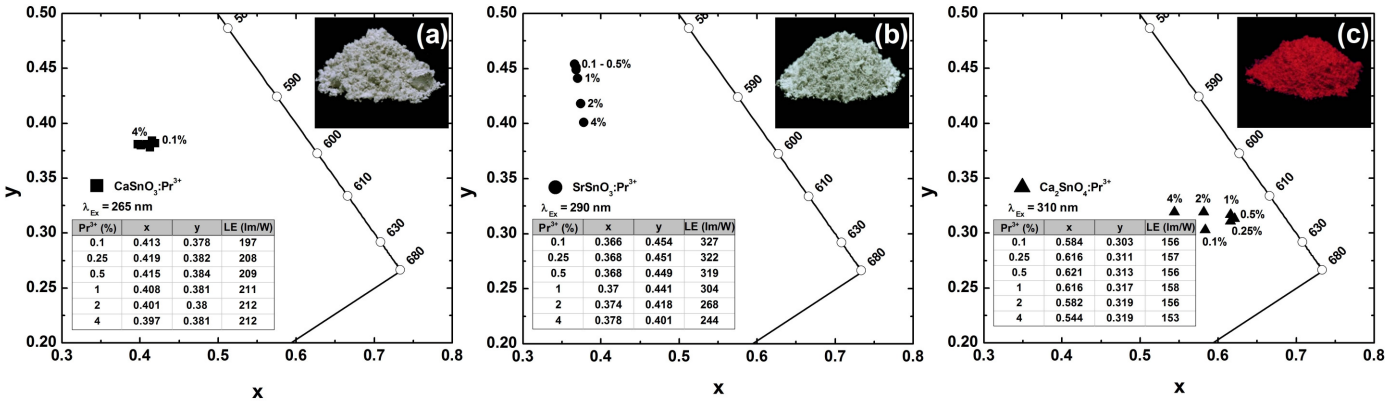

Pr^{3+} (%)	x	y	LE (lm/W)
0.1	0.413	0.378	197
0.25	0.419	0.382	208
0.5	0.415	0.384	209
1	0.408	0.381	211
2	0.401	0.38	212
4	0.397	0.381	212

Pr^{3+} (%)	x	y	LE (lm/W)
0.1	0.366	0.454	327
0.25	0.368	0.451	322
0.5	0.368	0.449	319
1	0.37	0.441	304
2	0.374	0.418	268
4	0.378	0.401	244

Pr^{3+} (%)	x	y	LE (lm/W)
0.1	0.584	0.303	156
0.25	0.616	0.311	157
0.5	0.621	0.313	156
1	0.616	0.317	158
2	0.582	0.319	156
4	0.544	0.319	153